Observation of Quantum Interference as a Function of Berry's Phase in a Complex Hadamard Optical Network

Anthony Laing,* Thomas Lawson, Enrique Martín López, and Jeremy L. O'Brien

Centre for Quantum Photonics, H. H. Wills Physics Laboratory & Department of Electrical and Electronic Engineering, University of Bristol, BS8 1UB, United Kingdom

(Received 15 February 2012; published 28 June 2012)

Emerging models of quantum computation driven by multiphoton quantum interference, while not universal, may offer an exponential advantage over classical computers for certain problems. Implementing these circuits via geometric phase gates could mitigate requirements for error correction to achieve fault tolerance while retaining their relative physical simplicity. We report an experiment in which a geometric phase is embedded in an optical network with no closed loops, enabling quantum interference between two photons as a function of the phase.

DOI: 10.1103/PhysRevLett.108.260505 PACS numbers: 03.67.Lx, 03.65.Vf, 42.50.Ar, 42.50.Xa

When a quantum mechanical system evolves under some Hamiltonian, the probability amplitudes associated with indistinguishable events can accumulate dynamical and geometric phases [1] and interfere constructively or destructively. In Hong Ou Mandel interference [2], when two photons meet at the input ports of a beam splitter, the event that both photons are transmitted is indistinguishable from the event that both photons are reflected, but the associated probability amplitudes have opposite phases and so interfere destructively: the probability to detect one photon at each output port is zero. This quintessentially *quantum* photonic interference generates the nonclassical correlations in multiphoton quantum walks [3,4] and the computational complexity of many-photon interference in large optical networks [5–7]. These emerging models of quantum computation are unlikely to be universal but may be exponentially more powerful than classical computers for certain problems. Crucially, since the basic models do not require initial entanglement, conditional gates, or feed-forward operations, large scale examples will be substantially less challenging to physically construct than a universal quantum computer. Achieving fault tolerance in these schemes without sacrificing their relative physical simplicity to unwieldy error correction is a key goal.

Geometric phases and, more generally, non-Abelian holonomies have been proposed as a method to implement fault-tolerant gates for *universal* quantum computation [8–11], since they are robust against perturbations to which the important global geometric properties are invariant [12–17]. As described by Berry [1], a phase is accrued by a vector in an instantaneous eigenstate of a Hamiltonian undergoing cyclic adiabatic evolution. Anticipated in an earlier classical result [18] and verified experimentally [19–21], the geometric phase has undergone important generalizations, including the non-Abelian [22] and nonadiabatic cases [23], the noncyclic [24–26] and nonunitary [27] cases, and the case where the endpoints of the evolution are orthogonal [28–30]. The geometric phase has been observed at the single photon level and in the context of nonlocality [31–33], while a biphoton wave packet in a superposition of modes in a closed interferometer exhibits the predicted increase in sensitivity to a geometric phase [34–36] that is observed for a dynamical phase [37]. To date, however, all observations of optical geometric phases involve self-interference of a single photon or classical light interference.

In light of the computational attributes of quantum interference between different photons and the desire to achieve fault tolerance in physically feasible computational models driven by this effect, demonstrating exquisite control over photonic quantum interference via an intrinsically robust geometric phase gate is a key step. Such an experimental connection in the context of these models is somewhat analogous to the implementation of a holonomic two-qubit gate in the established circuit model of universal quantum computation. Furthermore, to directly observe the influence of the geometric phase on interference between photons, any measurement statistics should not be obfuscated by other phase-dependent phenomena. In particular, single-photon interference, which has already been demonstrated to be predictably receptive to the geometric phase, should ideally be independent from the geometric phase in such an observation.

Here, we establish an experimental functional relationship connecting a variable geometric phase (VGP) to sinusoidal quantum interference between individual photons of a pair. The VGP is imparted inside a four-mode optical network that contains no closed loops, such that no single-photon interference can take place. Applied to only one photon of the pair in one of the modes, the VGP arises through a traversal of the polarization sphere comprising a closed cycle and an open path; the end points of the total traversal are mutually orthogonal. The other three modes traverse lengths on the polarization sphere equal to that of the VGP mode, but these include a partial, or total, path retracing such that a fixed GP, or no GP, is finally imparted.

Polarization vectors evolve via parallel transport, ensuring zero dynamical phase here, while the unknown dynamical phase contributions from small physical length mismatches are fixed. We observe high visibility quantum interference fringes and find an approximate flat line response for one-photon inputs, confirming the absence of single-photon interference.

Complex Hadamard matrices [38] relate the computational basis of a discrete Hilbert space to some mutually unbiased basis [39]. The four-mode complex Hadamard unitary, H_4, transforms quantum states according to

$$H_4 = \frac{1}{2}\begin{pmatrix} 1 & 1 & 1 & 1 \\ 1 & e^{i\theta} & -1 & -e^{i\theta} \\ 1 & -1 & 1 & -1 \\ 1 & -e^{i\theta} & -1 & e^{i\theta} \end{pmatrix}$$

so that a single particle prepared in a well-defined position corresponding to an element of the computational basis, when acted upon by a device described by H_4, emerges with maximal uncertainty in its position. A large ensemble of similarly prepared one-particle input states will be found after the device with approximately one quarter of their total number at each of the four detectors (in the case of no losses). Modulation of the phase θ in the H_4 device has no consequence for the maximal uncertainty in position of the single particle and no consequence for the detection statistics of the ensemble.

The optical network shown schematically in Fig. 1(a) consists of four one-half reflectivity beam splitters, a swap of the two middle modes, a phase shift θ on the lowest mode, and four detectors (D_i); it is equivalent to H_4 with the labeling of input and output ports indicated. The network contains no closed-loop interferometers, and a photon injected into any input port emerges in an equal superposition of the four output ports, regardless of the phase setting. Similarly, measurement in the computational basis of one-photon ensembles cannot reveal any information about θ, and these statistics should ideally give a flat-line response to modulation of this phase.

The situation is dramatically different for two-photon input states. Simultaneous injection into the complex Hadamard network of a photon in mode $|0\rangle$ and a photon in mode $|1\rangle$ leads to a state that experiences photonic quantum interference, producing correlations between pairs of detectors as a function of θ. The conditional probabilities for coincidental detection of photons are summarized in Eq. (1). Given a detection at D_i, the probability $\Pr(j \mid i)$ for a detection D_j is

$$\Pr(i \pm 1[\mathrm{mod}4] \mid i = \{0, 2\}) = (1 \pm \cos\theta)/2,$$
$$\Pr(i + 2 \mid i = \{0, 1\}) = 0. \quad (1)$$

Implementing θ geometrically creates a system in which quantum correlations from two-photon inputs are a function of a geometric phase, whereas its effects are unobservable in statistics from one-photon inputs, which would not be the case in an interferometer such as the Mach Zehnder.

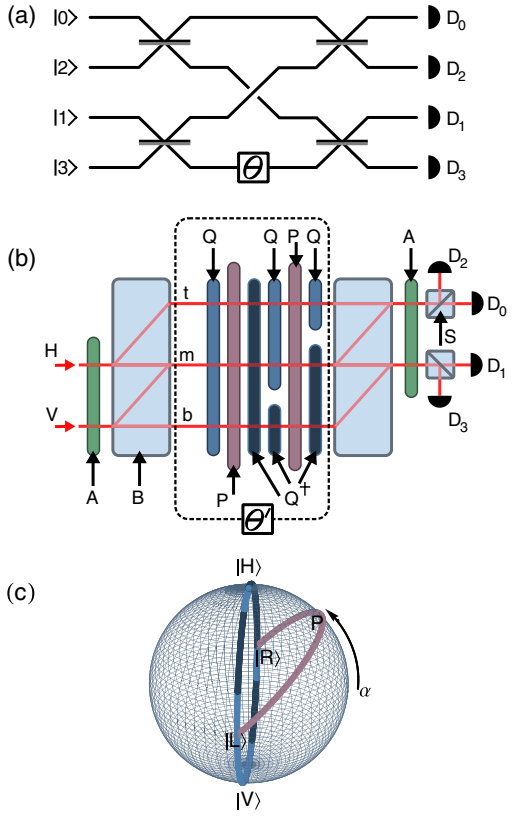

FIG. 1 (color online). Complex Hadamard network and VGP. (a) Schematic of the optical network, with phase shift θ. (b) Experimental construction based on beam displacers, with wave plates implementing a geometric phase θ'. (c) Sphere showing stages of polarization vector travel in the θ' section.

Devices implementing discrete instances of transformations similar to H_4 have been constructed in bulk optics for a small number of *dynamical* phase settings [40] and in multimode waveguides [41] where the phase is permanently fixed at a single value. Here, we encode in position (rail) and polarization, using a pair of parallelized Jamin-Lebedeff interferometers in a calcite beam displacer architecture, as shown in Fig. 1(b), to construct a device equivalent to H_4 up to trivial phases on input and output ports and relabeling [42]. Expanding to six modes through the θ' section, we use an arrangement of wave plates to implement the phase geometrically, allowing continuous transition between all phase values. The action of the beam splitters in Fig. 1(a) is equivalently implemented on polarization by half wave plates (A) with optic axes set to 22.5°; the swap is facilitated with beam displacers (B) that force horizontally polarized light to walk off at an angle, while vertically polarized light continues undeviated; polarization beam splitters (S) convert polarization to position for detection.

The θ' section in Fig. 1(b) comprises quarter wave plates with optic axes fixed at 45° (Q), or at −45° ($Q^\dagger$), and half wave plates (P) free to rotate but with optic axes locked

together at the same angle α. Overall, this implements a polarization flip on the top rail (t), the identity on the middle rail (m) [43], while the bottom rail (b) experiences a polarization flip *and* a VGP as a function of α. Figure 1(c) shows the polarization sphere [44]. Photons in rails t and m retrace their polarization steps from the halfway point; while the total path length traversed on the polarization sphere for light in rail b is equal to that of rails t and m, the crucial difference in the actual route traversed leads to the experimental VGP, $\theta'(\alpha)$.

The polarization vector in rail b, of light traveling the θ' section of Fig. 1(b), makes a traversal of the sphere of Fig. 1(c) that includes a closed cycle and an open path. The full traversal is VRP(α)LHRP(α)LH, with $P(\alpha)$ indicating a point on the sphere determined by the variable angle of the half wave plates. The respective $SU(2)$ unitaries for the polarization vectors of the three rails are

$$U_t = i\begin{pmatrix} 0 & 1 \\ 1 & 0 \end{pmatrix}, \quad U_m = \begin{pmatrix} 1 & 0 \\ 0 & 1 \end{pmatrix}, \quad U_b = i\begin{pmatrix} 0 & e^{i4\alpha} \\ e^{-i4\alpha} & 0 \end{pmatrix},$$

where $|H\rangle \equiv |0\rangle$ and $|V\rangle \equiv |1\rangle$ in each subspace. In this construction, a 1° change in the synchronized optic axes of both rotatable half wave plates results in a 4° shift in the experimental geometric phase: $4\Delta\alpha = \Delta\theta'$. Light in rails t and b receive a polarization flip during the full traversal so that the initial and final polarization vectors of the respective rails are orthogonal. Interestingly, a geometric phase is accrued in this situation [28] and can be identified as the fixed i factor on these unitaries.

To observe the correlations predicted in Eq. (1), pairs of photons were injected into the network as shown in Fig. 1(b): a horizontally polarized photon into rail m, and a vertically polarized photon into rail b, corresponding to computational states $|0\rangle$ and $|1\rangle$ respectively. The P wave plates were rotated almost two full revolutions, scanning a near $8 \times 2\pi$ range for θ'. To confirm the insensitivity of one-photon statistics to $\Delta\theta'$, one photon was injected into the network, for each of the $|0\rangle$ and $|1\rangle$ inputs, with another photon sent directly to a detector, as a herald. Photons were generated in a spontaneous parametric down-conversion source [45].

Experimental data shown in Fig. 2 strongly support predictions from Eq. (1). Figure 2(a) displays raw data for all six coincidence counts, with the expected four high visibility quantum interference fringes—the difference in amplitudes is due to different coupling efficiencies. In contrast, the two signals from detectors D_0-D_2 on rail t [upper pane in Fig. 2(a)], and D_1-D_3 on rail m [lower pane

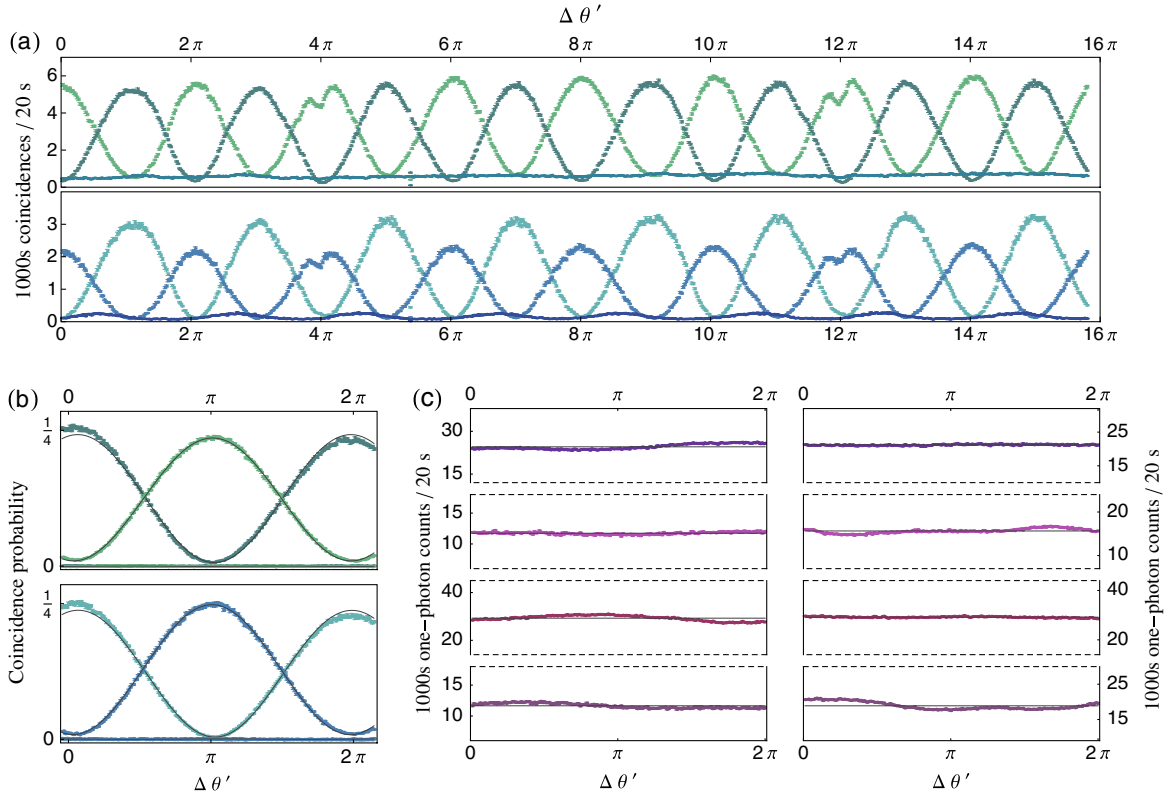

FIG. 2 (color online). Photonic quantum interference and one-photon response to the change in experimental geometric phase θ'. (a) Raw data for all six coincidence outputs showing quantum interference as a function of $\Delta\theta'$. (b) The four $\Delta\theta'$ sensitive quantum signals for a 2π range of the geometric phase, normalized. (c) Raw data for all eight output signals for both individual one-photon inputs.

in Fig. 2(a)] show the predicted continuous and near total destructive quantum interference, with negligible response to $\Delta\theta'$; the greatest phase response of these two signals was D_1-D_3 with a $0.9 \pm 0.1\%$ amplitude [46].

Coincidence counts for the four $\Delta\theta'$ quantum response curves were retaken over the 2π range shown in Fig. 2(b) and normalized for the measured coupling efficiencies. Following the notation from Eq. (1), the upper pane in Fig. 2(b) shows $\Pr(1 \mid 0)$ and $\Pr(1 \mid 2)$ with a respective minimum and maximum at π radians; the lower pane in Fig. 2(b) shows $\Pr(3 \mid 2)$ and $\Pr(3 \mid 0)$ with a respective minimum and maximum at π radians. The average visibility of these fringes is $94.0 \pm 0.2\%$ given from the fit that is shown as a solid black line. The small flat data in Fig. 2(b) are respective *accidental* signals, which are taken into account for the visibility calculation [47]. The raw data in Figure 2(c) confirm the insensitivity of one-photon statistics to $\Delta\theta'$. The four panes on the left of Fig. 2(c) show plots taken with a photon input in state $|0\rangle$ with the top plot showing data for detector D_0, the next plot below showing data for D_1, and so on; similarly the plots on the right of Fig. 2(c) are taken for input state $|1\rangle$. In each case the average count is shown as the solid line and the phase insensitivity is quantified by the relative standard error (RSE) from this line. The average RSE from all eight plots is 3%; the plot with the greatest RSE at 6% is from detector D_3 with input state $|1\rangle$.

The polarization operations in the θ' section of Fig. 1(b) give zero dynamical phase contributions if the polarization vectors are parallel transported at all times. The condition for parallel transport, for a certain state vector $|\psi(t)\rangle$, is $\langle\psi(t)|\dot{\psi}(t)\rangle = 0$, which implies that, at an infinitesimal time step later, the state $|\psi(t + \delta t)\rangle$ remains in phase with $|\psi(t)\rangle$. This condition is met for individual single-photon states and for the composite two-photon state superposed across all three rails of the θ' section in Fig. 1(b). The lengths of rails t, m, and b are not matched on the wavelength scale of the photons so that unknown dynamical phase differences occur between these rails, which are fixed due to the intrinsic stability of the experimental architecture. Therefore, the only variable phase is that on rail b and is a function of the common adjustable angle of the two P half wave plates.

We have observed photonic quantum interference fringes that are a function of a variable geometric phase. This direct observation of the Berry phase in the quantum signal is possible because the optical complex Hadamard network contains no closed loops, so does not support single-photon interferometry. All active elements of the state's Hilbert space make equal path length traversals on the polarization sphere, but only those elements of the two-photon state that traverse via a particular route lead to a variable geometric phase. This route comprises a full cycle and an open path on the polarization sphere, with mutually orthogonal start and end points. We have, therefore, simultaneously experimentally tested several important and distinct aspects of the geometric phase in conjunction with making the central quantum-interference observation of the Berry phase.

The experimental network reported here is a small scale example of a model of quantum computation driven by photonic quantum interference [4,7], with a holonomic component. Generalizations of holonomies have previously been widely investigated for robust gate operation in qubit-based universal quantum computation, as discussed, and theoretically examined in the specific case of photonic qubits [48]. Aside from imperfect unitary operation, the other major source of error in current linear optical experiments is typically photon loss; however, evidence suggests that loss in these models can be compensated through the injection of higher numbers of photons [49]. Furthermore, holonomies may reduce the exposure of photons to mode mismatch, leading to less demand on filtering, thus reducing loss.

Scaling up examples of holonomic multiphoton-interference-driven computational models in waveguides [50] where dynamical logic gates have been shown to work with high fidelity [51] is an appealing prospect. Any unitary transformation on modes can be implemented with a network of Mach Zehnder interferometers [52] which have been realized in waveguides with variable thermo-optic [53] and electro-optic [54] phase shifts and integrated into a partially reconfigurable on-chip logic gate [55]. An interesting line of research is to consider the class of holonomic operations available given a large-scale fully reconfigurable optical unitary network and the extent to which the global properties are invariant to imperfect splitting ratios in directional couplers and small random fluctuations from voltage-controlled phase shifters, which act locally.

We thank S. Bartlett, N. Brunner, J. Carolan, F. Flicker, M. Lobino, J. Matthews, K. Poulios, N. Russell, and P. Shadbolt for helpful discussions. This work was supported by EPSRC, ERC, PHORBITECH, and NSQI. J. L. O'B. acknowledges a Royal Society Wolfson Merit Award.

*anthony.laing@bristol.ac.uk

[1] M. V. Berry, Proc. R. Soc. London A **392**, 45 (1984).
[2] C. K. Hong, Z. Y. Ou, and L. Mandel, Phys. Rev. Lett. **59**, 2044 (1987).
[3] Y. Bromberg, Y. Lahini, R. Morandotti, and Y. Silberberg, Phys. Rev. Lett. **102**, 253904 (2009).
[4] A. Peruzzo, M. Lobino, J. C. F. Matthews, N. Matsuda, A. Politi, K. Poulios, X.-Q. Zhou, Y. Lahini, N. Ismail, K. Wörhoff, and *et al.*, Science **329**, 1500 (2010).
[5] L. G. Valiant, Theor. Comput. Sci. **8**, 189 (1979).
[6] S. Scheel, arXiv:quant-ph/0406127v1.
[7] S. Aaronson and A. Arkhipov, in *QIP 2010: The 13th Workshop on Quantum Information Processing* (ETC, Zurich, 2010).

[8] P. Zanardi and M. Rasetti, Phys. Lett. A **264**, 94 (1999).
[9] J. Pachos, P. Zanardi, and M. Rasetti, Phys. Rev. A **61**, 010305 (1999).
[10] J. A. Jones, V. Vedral, A. Ekert, and G. Castagnoli, Nature **403**, 869 (2000).
[11] L.-M. Duan, J. I. Cirac, and P. Zoller, Science **292**, 1695 (2001).
[12] A. Carollo, I. Fuentes-Guridi, M. F. Santos, and V. Vedral, Phys. Rev. Lett. **90**, 160402 (2003).
[13] G. De Chiara and G. M. Palma, Phys. Rev. Lett. **91**, 090404 (2003).
[14] A. Carollo, I. Fuentes-Guridi, M. F. Santos, and V. Vedral, Phys. Rev. Lett. **92**, 020402 (2004).
[15] P. Solinas, P. Zanardi, and N. Zanghì, Phys. Rev. A **70**, 042316 (2004).
[16] I. Fuentes-Guridi, F. Girelli, and E. Livine, Phys. Rev. Lett. **94**, 020503 (2005).
[17] S. Filipp, J. Klepp, Y. Hasegawa, C. Plonka-Spehr, U. Schmidt, P. Geltenbort, and H. Rauch, Phys. Rev. Lett. **102**, 030404 (2009).
[18] S. Pancharatnam, Proc. Ind. Acad. Sci. A **44**, 247 (1956).
[19] A. Tomita and R. Y. Chiao, Phys. Rev. Lett. **57**, 937 (1986).
[20] T. H. Chyba, L. J. Wang, L. Mandel, and R. Simon, Opt. Lett. **13**, 562 (1988).
[21] P. J. Leek, J. M. Fink, A. Blais, R. Bianchetti, M. Gppl, J. M. Gambetta, D. I. Schuster, L. Frunzio, R. J. Schoelkopf, and A. Wallraff, Science **318**, 1889 (2007).
[22] F. Wilczek and A. Zee, Phys. Rev. Lett. **52**, 2111 (1984).
[23] Y. Aharonov and J. Anandan, Phys. Rev. Lett. **58**, 1593 (1987).
[24] T. F. Jordan, Phys. Rev. A **38**, 1590 (1988).
[25] Y.-S. Wu and H.-Z. Li, Phys. Rev. B **38**, 11907 (1988).
[26] H. Weinfurter and G. Badurek, Phys. Rev. Lett. **64**, 1318 (1990).
[27] J. Samuel and R. Bhandari, Phys. Rev. Lett. **60**, 2339 (1988).
[28] N. Manini and F. Pistolesi, Phys. Rev. Lett. **85**, 3067 (2000).
[29] H.-M. Lauber, P. Weidenhammer, and D. Dubbers, Phys. Rev. Lett. **72**, 1004 (1994).
[30] Y. Hasegawa, R. Loidl, M. Baron, G. Badurek, and H. Rauch, Phys. Rev. Lett. **87**, 070401 (2001).
[31] P. G. Kwiat and R. Y. Chiao, Phys. Rev. Lett. **66**, 588 (1991).
[32] D. V. Strekalov and Y. H. Shih, Phys. Rev. A **56**, 3129 (1997).
[33] M. Ericsson, D. Achilles, J. T. Barreiro, D. Branning, N. A. Peters, and P. G. Kwiat, Phys. Rev. Lett. **94**, 050401 (2005).
[34] D. Klyshko, Phys. Lett. A **140**, 19 (1989).
[35] J. Brendel, W. Dultz, and W. Martienssen, Phys. Rev. A **52**, 2551 (1995).
[36] H. Kobayashi, Y. Ikeda, S. Tamate, T. Nakanishi, and M. Kitano, Phys. Rev. A **83**, 063808 (2011).
[37] J. G. Rarity, P. R. Tapster, E. Jakeman, T. Larchuk, R. A. Campos, M. C. Teich, and B. E. A. Saleh, Phys. Rev. Lett. **65**, 1348 (1990).
[38] W. Tadej and K. Życzkowski, Open Syst. Inf. Dyn. **13**, 133 (2006).
[39] T. Durt, B.-G. Englert, I. Bengtsson, and K. Życzkowski, Int. J. Quant. Inform. **08**, 535 (2010).
[40] K. Mattle, M. Michler, H. Weinfurter, A. Zeilinger, and M. Zukowski, Appl. Phys. B **60**, S111 (1995).
[41] A. Peruzzo, A. Laing, A. Politi, T. Rudolph, and J. L. O'Brien, Nat. Commun. **2**, 224 (2011).
[42] Labeling a horizontally (vertically) polarized photon with $H(V)$, and a photon in the middle (bottom) rail with $m(b)$, the computational basis on inputs follows as $|0\rangle \equiv |H, m\rangle$, $|1\rangle \equiv |V, b\rangle$, $|2\rangle \equiv |V, m\rangle$, and $|3\rangle \equiv |H, b\rangle$. Output labeling is indicated by detector subscripts.
[43] The effective operation on the top and middle rails can easily be seen by noting that the two innermost quarter wave plates are mutually conjugate and, together, implement the identity. Outside of these, the two half wave plates at the same angle also implement the identity, since a half wave plate gives an Hermitian operation. Then the outermost quarter wave plates implement the polarization flip (and fixed phase) on the top rail, and the identity on the middle rail.
[44] Similar to the Bloch sphere or Poincaré sphere, canonical labeling on the sphere of light polarization follows $H(V) \equiv$ horizontal(vertical), $D(A) \equiv$ diagonal(anti-diagonal), and $R(L) \equiv$ right(left)circular.
[45] A 2 mm thick bismuth triborate crystal cut for Type 1 phase matching was pumped with a 404 nm wavelength continuous wave laser, focused to a 40 μm waist. Photons were collected, after passing through 2 nm interference filers, into polarization maintaining optical fibres, and injected into the experimental network.
[46] This amplitude was calculated by taking the difference between the visibilities in the Hong Ou Mandel dips for the $\theta' = 0$ and $\theta' = \pi$ cases.
[47] Accidental coincidence counts arise when the spontaneous parametric down conversion process (with a continuous wave pump) produces two photon pairs within the time resolution of the coincidence counter. This rate can be directly measured by introducing a delay to omit all *real* coincidences.
[48] K.-P. Marzlin, S. D. Bartlett, and B. C. Sanders, Phys. Rev. A **67**, 022316 (2003).
[49] P. P. Rohde and T. C. Ralph, Phys. Rev. A **85**, 022332 (2012).
[50] A. Politi, M. J. Cryan, J. G. Rarity, S. Yu, and J. L. O'Brien, Science **320**, 646 (2008).
[51] A. Laing, A. Peruzzo, A. Politi, M. R. Verde, M. Halder, T. C. Ralph, M. G. Thompson, and J. L. O'Brien, Appl. Phys. Lett. **97**, 211109 (2010).
[52] M. Reck, A. Zeilinger, H. J. Bernstein, and P. Bertani, Phys. Rev. Lett. **73**, 58 (1994).
[53] J. C. F. Matthews, A. Politi, A. Stefanov, and J. L. O'Brien, Nat. Photonics **3**, 346 (2009).
[54] D. Bonneau, M. Lobino, P. Jiang, C. M. Natarajan, M. G. Tanner, R. H. Hadfield, S. N. Dorenbos, V. Zwiller, M. G. Thompson, and J. L. O'Brien, Phys. Rev. Lett. **108**, 053601 (2012).
[55] P. J. Shadbolt, M. R. Verde, A. Peruzzo, A. Politi, A. Laing, M. Lobino, J. C. F. Matthews, M. G. Thompson, and J. L. O'Brien, Nat. Photonics **6**, 45 (2012).